Geomagnetic Sensor based Abnormal Parking Detection in Smart Roads

Runsen He[1,2], Guoqiang Mao[1,2], Yilong Hui[1,2,*], and Qingwei Cheng[1,2]
1.State Key Laboratory of Integrated Services Networks, Xidian University, Xi'an, 710071
2.Research Institute of Smart Transportation, Xidian University, Xi'an, 710071
*ylhui@xidian.edu.cn

***Abstract*—With the development of Internet of Things (IoT) and communication technology, abnormal parking detection based on geomagnetic sensors equipped with solar panels has become increasingly feasible and important. False parking detection is a main challenge affecting the widespread use of the aforementioned technology. Especially when ambient light change triggers changes in the current of solar panel, which may in turn cause local EM field changes and affect the detection of nearby geomagnetic sensor. To that end, we propose an abnormal parking detection scheme to distinguish between real parking and false detections. Specifically, we establish an equivalent model of the magnetic field around the solar panel, and design a method to compute the magnetic field at the periphery of the solar panel. Then, we analyze the difference between the magnetic field caused by the changes in ambient light and the magnetic field produced by vehicles, and extract features that distinguish abnormal parking from false detections. Based on the features, a state machine is designed to distinguish the false detection of light from the real parking based on the magnetic field waveform. Field tests show that the accuracy of the designed abnormal parking detection scheme can reach 97%.**

***Index Terms*—Internet of things, abnormal parking detection, geomagnetic sensor, smart roads**

I. Introduction

With the rapid development of Internet of Things (IoT) and communication technology, smart road technology has received extensive attention from industry and academia [1]. In smart roads, by analyzing and processing traffic data sensed by roadside sensors, efficient traffic management and abnormal event processing can be achieved to improve the traffic efficiency.

As a common road abnormal event, abnormal parking refers to an event in which vehicles stay on the main lane or emergency lane. Due to the high driving speed of vehicles, abnormal parking events will affect the normal traffic order and may lead to traffic accidents. Therefore, accurate identification of abnormal vehicle parking events is an important function for smart roads. The existing schemes for detecting abnormal parking based on various radars or videos are difficult to deploy on a large scale on highways due to cost limitations or visibility limitations. Recently, due to the advantages of geomagnetic sensors such as low cost and robust to environmental changes, researchers worldwide have investigated parking detection schemes based on geomagnetic sensors. In [2], the authors proposed an intelligent vehicle management scheme using geomagnetic sensors to realize real-time sharing of parking space information. In [3], the authors proposed a parking detection algorithm for eliminating interference from adjacent parking. The test showed that the detection accuracy of the algorithm for vehicles entering and leaving the parking space is 99.8% and 99.9%, respectively. In order to overcome the interference of vehicles in adjacent parking spaces, Zhang et al. [4] fused the data features collected by the geomagnetic sensors from multiple adjacent parking spaces to detect the current parking space occupancy. In [5], the authors proposed a parking detection algorithm that considers the temperature drift. With this algorithm, the influence of temperature on parking detection accuracy can be reduced.

Although parking detection based on geomagnetic sensors has been widely studied, the detection solutions in the literature mostly focused on detection in parking lots, with few studying abnormal parking detection in highways. In the parking lot scenario, the number of sensors is relatively small and the location is relatively concentrated. Therefore, the sensors can be powered by the battery or directly connected to a power source. However, in the highway scenario, the replacement of batteries or wired power supply will bring huge consumption of human and financial resources.

For this reason, IoT devices integrating solar panels and geomagnetic sensors have gradually gained widespread attention [6]. Through the integration of geomagnetic sensors, microprocessors, solar panels, batteries and other components, the sensors can overcome the problems of high manufacturing costs and poor battery life, and realize real-time abnormal parking detection in highway scenarios. However, the integration of solar panels and geomagnetic sensors in closely packed IoT devices also brings new challenges. Specifically, when the solar panel charges the sensor battery under sunlight, a photon-generated current will be generated, which induces magnetic field around the solar panel. Therefore, when the ambient light changes drastically, the magnetic field strength around the solar panel will fluctuate, which may cause false detection and affect the accuracy of traffic flow monitoring [7].

To address the aforementioned false detection problem, we propose an abnormal parking detection scheme that can distinguish between real parking and false detection. Specifically, we first establish a magnetic field model around

GLOBECOM 2023 - 2023 IEEE Global Communications Conference | 979-8-3503-1090-0/23/$31.00 ©2023 IEEE | DOI: 10.1109/GLOBECOM54140.2023.10437955

Authorized licensed use limited to: XIDIAN UNIVERSITY. Downloaded on December 11,2024 at 05:22:40 UTC from IEEE Xplore. Restrictions apply.

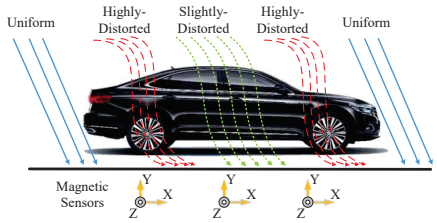

Fig. 1. The deployment of sensor node

the solar panel to calculate the magnetic field at the periphery of the solar panel. Then, we analyze the difference between the magnetic field generated by light and the magnetic field generated by a vehicle passing through the geomagnetic sensor, and extract the features that can be used to distinguish abnormal parking and false detection. After that, we design a state machine to distinguish between false detections caused by the changes in ambient light and real parking. Finally, we verify the effectiveness of our proposed scheme through field tests.

The remainder of this paper is summarized as follows. Section II presents the system model of the geomagnetic sensor node and the equivalent model of the magnetic field around the solar panel. In Section III, the abnormal parking detection scheme is described. Section IV presents the experimental results, followed by the conclusion in Section V.

II. System Model

A. Geomagnetic Sensor

The geomagnetic sensor node used in this paper is composed of microprocessor, geomagnetic sensor, data transmission module, solar panel, battery and its charging circuit [8].

The microprocessor adopts STM32F103 series 64-bit microcontroller. The solar panel converts solar energy into electrical energy, charges the battery, which in turn supplies power to the sensor node. The geomagnetic sensor is a three-axis geomagnetic sensor with a sampling frequency of 100Hz. It can simultaneously collect three-axis (i.e, X, Y, Z) magnetic field strength data. After collecting the data, the data transmission module then uses the LoRa wireless communication module to upload the data to an edge computing server. As shown in Fig. 1, the sensor nodes are deployed along the road boundary line, where the positive direction of the X-axis of the sensor is the same as the driving direction of the vehicle; the positive direction of the Y-axis is parallel to the road and points to the centre of the lane; the positive direction of the Z-axis is perpendicular to the road.

Let $F_x(k)$, $F_y(k)$, and $F_z(k)$ denote the magnetic field data of the X, Y, and Z axes at the k-th sampling instant. In order to process the environmental noise, the collected data will be processed by a moving average filter. The filtering formula can be expressed as

$$\overline{F_i(k)} = \frac{1}{W-2}\left(\sum_{j=1}^{W} F_i(k-W+j) - F_{\min} - F_{\max}\right) \tag{1}$$

where $i \in \{X, Y, Z\}$, $\overline{F_i(k)}$ is the filtered data, W is the length of the sliding window, $F_{\min}$ and $F_{\max}$ are the minimum and maximum values of the magnetic field data in the sliding window, respectively [8].

As shown in Fig. 1, when the vehicle enters the detection range of the geomagnetic sensor, the vehicle will induce a magnetic field which can be sensed by the geomagnetic sensor. When the vehicle leaves the detection range of the geomagnetic sensor, the surrounding magnetic field will return to the original level. Therefore, we take the magnetic field strength value when no vehicle passes as the baseline. If the detected magnetic field strength deviates significantly from the baseline, it indicates that the vehicle is entering. Conversely, if the magnetic field strength returns to the vicinity of the baseline, it indicates that the vehicle is leaving. Since the geomagnetic field will fluctuate slowly due to the interference of environmental factors such as temperature, the sensor nodes will update the baseline when no vehicles pass by. We have

$$F_b^i = \frac{1}{J}\sum_{j=1}^{J} F_i(k-J+j) \tag{2}$$

where F_b^i is the updated baseline on axis i, which is equal to the average of the latest J raw data collected for this axis.

In order to make full use of the information of the three-axis data, the microprocessor fuses the filtered three-axis data and uses the fused data for vehicle detection [8]. The three-axis data can be fused by

$$F_{fusion}(k) = \sqrt{\left(\overline{F_X(k)} - F_b^X\right)^2 + \left(\overline{F_Y(k)} - F_b^Y\right)^2 + \left(\overline{F_Z(k)} - F_b^Z\right)^2} \tag{3}$$

where $F_{fusion}(k)$ is the fused magnetic field strength at sampling time k.

Based on (3), we set the detection threshold θ_{th}. If a consecutive of M sampled data satisfying $F_{fusion}(k) \geq \theta_{th}$, it is determined that a vehicle is passing the sensor node. In contrast, if a consecutive of N sampled data satisfying $F_{fusion}(k) < \theta_{th}$, it is determined that the vehicle has left.

B. Magnetic Field Model for Solar Panels

It has been pointed out in [9] that a direct current (DC) photon-generated current will be generated if sunlight hits a solar panel, which will induce a magnetic field in the space. Due to the large number of current branches on the surface of solar panels, analyzing the magnetic field intensity generated by each branch at a certain point in space is extremely cumbersome. Therefore, in order to simplify the calculation, we approximate and simplify multiple currents. Due to the symmetry of the solar panel circuit, we consider equating the photon-generated current inside it to a total current located

Authorized licensed use limited to: XIDIAN UNIVERSITY. Downloaded on December 11,2024 at 05:22:40 UTC from IEEE Xplore. Restrictions apply.

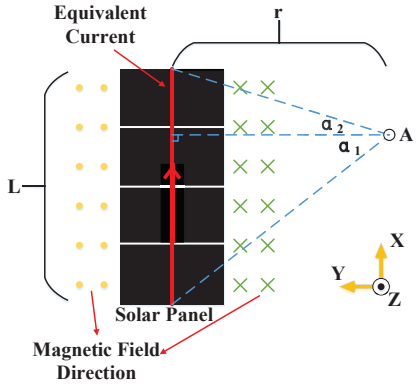

Fig. 2. The positional relationship between the solar panel and the geomagnetic sensor

at the centerline of the solar panel. Furthermore, we consider the geomagnetic sensor located at a point outside and near the solar panel. Then the positional relationship between the solar panel and the geomagnetic sensor can be simplified as the positional relationship between a finite-length DC current and a point outside the current, as shown in Fig. 2.

In Fig. 2, the photon-generated current inside the solar panel is approximately modeled by a DC current with a length L and a magnitude of I, where L is approximately equal to the length of the solar panel. Point A is the location of the geomagnetic sensor. r is the length of the vertical line from point A to the DC current I. By connecting point A to the two end points of the current, we can obtain the angles between the two lines and the vertical line, namely, α_1 and α_2. Let the vertical line be the reference and take the counterclockwise direction as the positive direction, then we have $\alpha_1 > 0$ and $\alpha_2 < 0$.

According to the electromagnetic field theory, the magnetic field strength generated by the equivalent current at point A in Fig. 2 is given by

$$\mathbf{B} = \frac{\mu_0 I}{4\pi} \int_L \frac{d\mathbf{L} \times \mathbf{r}}{r^3} = \mathbf{e} \cdot \frac{\mu_0 I}{4\pi r} (\sin\alpha_1 - \sin\alpha_2) \tag{4}$$

where μ_0 is the magnetic permeability in the vacuum, $\mathbf{e}$ is a unit vector with the same direction as the direction of the magnetic field $\mathbf{B}$.

According to the theory of photovoltaic power generation, the photon-generated current in the solar panel is proportional to the ambient light intensity. Therefore, it can be assumed that the relationship between the photon-generated current I and the light intensity G is

$$I = p_1 G + p_2 \tag{5}$$

where p_1 and p_2 are the unknown constants to be determined.

By substituting Eq. (5) into Eq. (4), the relationship between the magnetic field intensity $\mathbf{B}$ and the light intensity G can be given by

$$\mathbf{B} = \mathbf{e} \cdot \frac{\mu_0 (p_1 G + p_2)}{4\pi r} (\sin\alpha_1 - \sin\alpha_2) \tag{6}$$

III. Parking Detection Scheme

A. Detection of Vehicle Parking and Departure

It has been pointed out in Section II-A that the vehicle detection uses Eq. (3) to fuse the data collected by the geomagnetic sensor to determine the arrival and departure of vehicles. Therefore, the abnormal parking detection also uses the characteristics of the three-axis waveform to determine the parking event. When a vehicle is parked within the detection range of the sensor node for a sufficiently long time, the magnetic field waveform collected by the geomagnetic sensor will tend to be stable. In addition, the relative position of the vehicle to the sensor node will result in different waveform shapes and amplitudes after stabilization.

Specifically, the range of magnetic field data is used in our scheme for judging whether the waveform becomes stable. Let F^S_{fusion} represents the set of S magnetic field data collected by the geomagnetic sensor, then the range of these data can be calculated by

$$Range = \max\{F^S_{fusion}\} - \min\{F^S_{fusion}\} \tag{7}$$

Based on Eq. (7), we denote the threshold as θ_{range}. If $Range < \theta_{range}$, it is determined that the waveform has stabilized. That is, a vehicle is parked within the detection range of the sensor node. The value of θ_{range} will be determined in Section III-D.

When the abnormally parked vehicle leaves, the magnetic field will return to a level similar to that before the vehicle parked. Therefore, similar to the detection of normal vehicles, the magnetic field strength of N consecutive sampled data is less than the detection threshold θ_{th}, it is determined that the vehicle has left, and the abnormal parking event ends.

B. Features to Distinguish False Detection from Real Parking

To distinguish between false detection caused by the changes in ambient light and real parking, we first need to analyze the difference between the two magnetic field waveforms. According to the research in [10], different parts of a vehicle have different degrees of influence on the geomagnetic field. Specifically, the parts that have the greatest influence on the geomagnetic field are mainly the axles and the engine. Therefore, we can divide abnormal parking into two cases according to different relative positions of the vehicle and the sensor node.

Case that has Not Passed(CNP): The vehicle stops as soon as it enters the detection range of the geomagnetic sensor, as shown in Fig. 3(a);

Case that has Passed(CP): Part or all of the vehicle has passed the geomagnetic sensor before stopping, as shown in Fig. 3(b).

For CNP, because the main body of the vehicle or the part that has a strong influence on the magnetic field is

Authorized licensed use limited to: XIDIAN UNIVERSITY. Downloaded on December 11,2024 at 05:22:40 UTC from IEEE Xplore. Restrictions apply.

(a) CNP (b) CP

Fig. 3. Two cases of abnormal parking

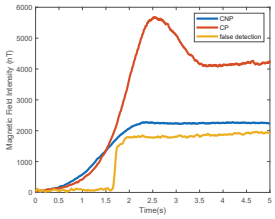

Fig. 4. The magnetic field waveforms of parking and false detection

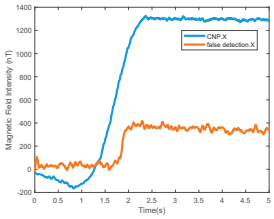

Fig. 5. The X-axis waveforms of CNP and of false detection in Fig. 4

gradually approaching the geomagnetic sensor, the magnetic field waveform shows an upward trend with time, and the amplitude of the overall waveform is however small, as shown in Waveform of CNP in Fig. 4. For CP, part or all of the vehicle that has a strong influence on the magnetic field begins to move away from the geomagnetic sensor. Thus, the magnetic field waveform has reached the peak value, and the amplitude begins to decrease, as shown in Waveform of CP in Fig. 4.

As can be seen from Fig. 4, the waveform of CP has a significant amplitude difference from the waveform of false detection. Therefore, we consider the "maximum value of the waveform" as a feature to distinguish false detection, which is represented by P_M. Specifically, when it is detected that the change of the current magnetic field may be caused by abnormal parking, by extracting the peak value of the waveform and comparing it with an appropriately chosen threshold θ_M, the false detection can be distinguished from the real parking in CP.

Different from CP, as shown in Waveform of CNP and Waveform of false detection in Fig. 4, the magnetic field waveform collected by the sensor node in CNP is similar to that caused by the false detection in amplitude and waveform. In this case, it is difficult to distinguish the false detection from the real parking using only P_M. To this end, we need to further consider other features. According to the model of the solar panel magnetic field in Section II-B, the direction of the magnetic field is perpendicular to the plane where the solar panel is located, that is, perpendicular to the X-axis of the geomagnetic sensor. Therefore, when the variation of illumination changes the magnetic field around the solar panel, the magnetic field mainly affects the Y-axis and Z-axis data of the geomagnetic sensor, and has less effect on the X-axis data. For the real parking event, when the sensor node detects the vehicle, the amplitudes of the magnetic field waveforms of the three axes have obvious changes. That is to say, the false detection mainly affects the data of the Y-axis and Z-axis of the geomagnetic sensor, and the abnormal parking has a relatively obvious impact on all three axes. Therefore, we can distinguish between abnormal parking and false detection by comparing the "change in amplitude of X-axis waveform", which is represented by Δx. Specifically, when the geomagnetic sensor detects a waveform suspected of abnormal parking, if the change of the waveform of the X-axis is less than a fixed threshold θ_x, it is considered that the waveform is generated by false detection. On the contrary, if the change of the waveform of the X-axis is greater than that, it is considered that the waveform is caused by real parking. Fig. 5 shows the X-axis waveforms of CNP and of false detection in Fig. 4, and it can be seen that there is a significant difference in amplitude between the two waveforms.

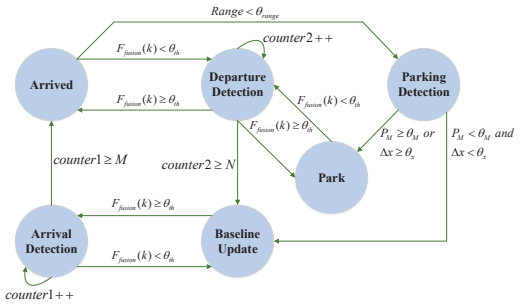

Fig. 6. State machine for abnormal parking detection

C. State Machine for Abnormal Parking Detection

According to the features discussed in Section III-B, the state machine for abnormal parking detection is shown in Fig. 6.

1) ***Baseline Update****:* When no vehicle passes by, the state machine is to update the baseline using Eq. (2); If $F_{fusion}(k) \geq \theta_{th}$, then jump to $Arrival\ Detection$ state.

2) ***Arrival Detection****:* In this state, a counter variable $counter1$ will be established to record the number of data satisfying $F_{fusion}(k) \geq \theta_{th}$. If $counter1 \geq M$, it suggests that a vehicle is coming, then the state jumps to $Arrived$ state; Once $F_{fusion}(k) < \theta_{th}$ is satisfied, then jump to $Baseline\ Update$ state.

3) ***Arrived****:* In this state, Eq. (7) will be used to periodically calculate $Range$. If $Range < \theta_{range}$, then jump to $Parking\ Detection$ state. If $F_{fusion} < \theta_{th}$, jump to $Departure\ Detection$ state;

4) ***Departure Detection****:* In this state, a counter $counter2$ will be established to record the number of data satisfying $F_{fusion} < \theta_{th}$. If $counter2 \geq N$, it indicates that the vehicle has left, then the state jumps to $Baseline\ Update$ state; Once $F_{fusion}(k) \geq \theta_{th}$ is satisfied, then jump to $Arrived$ state.

5) ***Parking Detection****:* In this state, the parameters P_M and Δx will be calculated to distinguish between false detection and parking events. If $P_M \geq \theta_M$ or $\Delta x \geq \theta_x$, then the state jumps to $Park$ state; If $P_M < \theta_M$ and

Authorized licensed use limited to: XIDIAN UNIVERSITY. Downloaded on December 11,2024 at 05:22:40 UTC from IEEE Xplore. Restrictions apply.

$\Delta x < \theta_x$, it means that it is a false detection, then jump to $Baseline\ Update$ state.

6) ***Park****:* In this state, the detection of vehicle departure is performed, where the detection method is the same as that of the $Arrived$ state.

D. Determination of Parameters

For threshold θ_{Range}, we assume that the ambient noise superimposed on the fused waveform follows a normal distribution with an expectation of 0 and a standard deviation of σ_{Range}. Then an estimate of the standard deviation $\widehat{\sigma}_{Range}$ can be obtained from the acquired waveform data. Based on $\widehat{\sigma}_{Range}$, we can take

$$\theta_{Range} = (4 \sim 6)\widehat{\sigma}_{Range} \tag{8}$$

When the range of the data is less than θ_{Range}, the current waveform can be considered to be stable.

For threshold θ_M, it is considered that its value should be equal to the maximum magnetic field change that can be generated by the false detection. Let $G_{\max}$ and $G_{\min}$ denote the maximum and minimum values of outdoor light intensity, respectively. Then, the value of θ_M can be calculated by

$$\theta_M = K \cdot \Delta G + p_2 \tag{9}$$

where $K = \frac{\mu_0 p_1}{4\pi r}(\sin\alpha_1 - \sin\alpha_2)$ and $\Delta G = G_{\max} - G_{\min}$.

For threshold θ_x, attributable to noise and modeling errors in the actual scene, the magnetic field strength on the X-axis caused by false detection cannot be completely 0. Therefore, based on the measured data, we count the variation of the X-axis magnetic field strength in the false detection data and use the maximum variation $\Delta\widehat{x}_{\max}$ as an estimate of the maximum magnetic field variation generated by the false detection on the X-axis. Then, we assume that the noise superimposed on the X-axis follows a normal distribution with an expectation of 0 and a standard deviation of σ_x. By collecting X-axis environmental data when no vehicles pass by, we can obtain the estimate of σ_x. Based on the estimate $\widehat{\sigma}_x$, we have

$$\theta_x = \Delta\widehat{x}_{\max} + (4 \sim 6)\,\widehat{\sigma}_x \tag{10}$$

For θ_{Range}, its value is related to $\widehat{\sigma}_{Range}$. In most road scenarios, there is no strong magnetic field interference source near the sensor node, and the noise mainly comes from the slight fluctuations of the geomagnetic field. Therefore, the value of $\widehat{\sigma}_{Range}$ is consistent across all scenarios. For θ_M and θ_x, K, p_2 and $\Delta\widehat{x}_{\max}$ involved in Eq. (9) and Eq. (10), they depend on the hardware properties of the sensor nodes. ΔG is the maximum value of outdoor light variation, which has fully considered the extreme situations in various road scenarios. θ_x is similar to θ_{Range}, and its value mainly depends on slight fluctuations in the geomagnetic field. Therefore, the values of θ_M and θ_x are not sensitive to different scenarios.

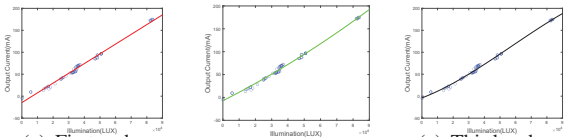

(a) First-order (b) Second-order (c) Third-order

Fig. 7. Polynomial fitting

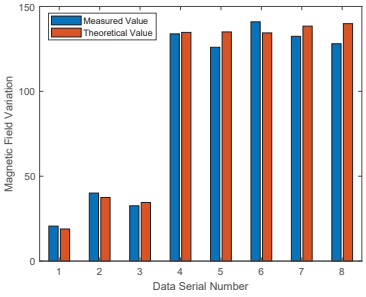

Fig. 8. Comparison of measured variation and theoretical variation

IV. Performance Evaluation

A. Magnetic Field Model Validation

We first verify the relationship between the photon-generated current in the solar panel and the ambient light intensity. We collected 60 sets of data, each of which includes ambient illuminance and the corresponding current output of the solar panel. Figs. 7(a)-7(c) show these collected data and the corresponding first-order, second-order and third-order polynomial fitting curves.

From these figures, it can be seen that the first-order polynomial can already reflect the relationship between illumination and output current well. When the order is increased, the fitting results obtained will not have significant improvement. Therefore, we can use Eq. (5) to characterize their relationship. In addition, by using the least square method, the parameters in Eq. (5) can be given by $p_1 = 0.002$ and $p_2 = -14.530$.

Based on Eq. (5), the rationality of Eq. (6) can be verified as follows. We collected 8 sets of data, where each set of data includes the variation of the ambient illuminance ΔG and the variation of the environmental magnetic field collected by the sensor node ΔB_m. By measuring the relative position of the solar panel and the geomagnetic sensor on the sensor node, we can obtain the values of r, $\sin\alpha_1$ and $\sin\alpha_2$ in Eq. (6) and further calculate the theoretical variation caused by the change in ambient illumination. Fig. 8 shows the values of ΔB_m and the theoretical variation of the data in the same set. It can be seen from Fig. 8 that the average relative error between the measured variation and the theoretical variation is 5.87%. Therefore, we can estimate the variation of magnetic field caused by illumination using Eq. (6).

B. Parking Detection Accuracy Test

To test the accuracy of the parking detection scheme, we deploy a sensor node on the lane line, as shown in Fig. 9.

Authorized licensed use limited to: XIDIAN UNIVERSITY. Downloaded on December 11,2024 at 05:22:40 UTC from IEEE Xplore. Restrictions apply.

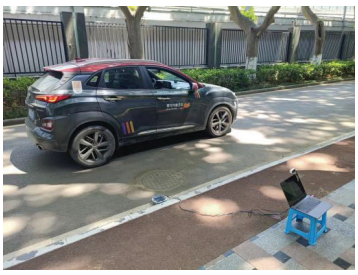

Fig. 9. Test scenario

TABLE I
DETECTION ACCURACY

Relative position of vehicle and sensor node	Lateral distance between vehicle and sensor node	Number of data sets	Detection Accuracy
CNP	0.3m	50	98%
	0.7m	50	98%
	1m	50	88%
CP	0.3m	50	100%
	0.7m	50	100%
	1m	50	98%

The raw geomagnetic field data collected by the sensor node in real time can be stored through the laptop. And we use a camera to record the actual situation of the test.

To calculate the detection rate of parking events, as shown in TABLE I, we consider different scenarios according to the relative position of the vehicle and the sensor node and the lateral distance between them. As can be seen from TABLE I, when the vehicle is close to the sensor node, the detection accuracy is high. However, when the distance reaches 1 meter, due to the obvious attenuation of the magnetic field, the amplitude of the magnetic field data collected by the sensor is small. Therefore, the detection accuracy decreases. Especially in CNP, when the lateral distance between the vehicle and the sensor node is equal to 1 meter, the detection rate is greatly reduced. This is because the distance between the vehicle and the sensor node in this case is the largest of the six cases in TABLE I. Due to the same amount of data in each scenario, taking the average of all accuracy rates in TABLE I can result in a detection accuracy of 97% for the parking detection scheme.

V. CONCLUSION

In this paper, an abnormal parking detection scheme based on geomagnetic sensor deployed in highway scenario is proposed. In order to improve the accuracy of abnormal parking detection, this paper focuses on the problem of false detection caused by the changes in ambient light. First, an equivalent magnetic field model around the solar panel is established. Then, we analyze the differences between the magnetic field changes caused by illumination and those caused by real parking, and propose an abnormal parking detection scheme to distinguish between false detection and real parking. The test results show that the magnetic field model of the solar panel can better reflect the real environmental magnetic field, and the accuracy of the designed algorithm is 97%.

For future work, we will comprehensively consider the influence of vehicle type and vehicle speed on the magnetic field waveform to further improve the performance of our parking detection scheme.

ACKNOWLEDGMENT

This research is supported by NSFC grant, Grant number: U21A20446.

REFERENCES

[1] G. Mao, Y. Hui, X. Ren, C. Li and Y. Shao, "The Internet of Things for Smart Roads: A Road Map From Present to Future Road Infrastructure," IEEE Intelligent Transportation Systems Magazine, early access, 2022.

[2] A. Floris, R. Girau, S. Porcu, G. Pettorru and L. Atzori, "Implementation of a Magnetometer based Vehicle Detection System for Smart Parking applications," 2020 IEEE International Smart Cities Conference (ISC2), 2020, pp. 1-7.

[3] H. Zhu, S. Feng and F. Yu, "Parking Detection Method Based on Finite-State Machine and Collaborative Decision-Making," in IEEE Sensors Journal, vol. 18, no. 23, pp. 9829-9839, Dec, 2018.

[4] Z. Zhang, X. Mao, K. Zhou and H. Yuan, "Collaborative Sensing-Based Parking Tracking System With Wireless Magnetic Sensor Network," in IEEE Sensors Journal, vol. 20, no. 9, pp. 4859-4867, May, 2020.

[5] J. Gu, Z. Zhang, F. Yu and Q. Liu, "Design and implementation of a street parking system using wireless sensor networks," IEEE 10th International Conference on Industrial Informatics, 2012, pp. 1212-1217.

[6] P. Šolić, A. Leoni, R. Colella, T. Perković, L. Catarinucci and V. Stornelli, "IoT-Ready Energy-Autonomous Parking Sensor Device," IEEE Internet of Things Journal, vol. 8, no. 6, pp. 4830-4840, 15 March, 2021.

[7] D. Norte, "Estimating Electromagnetic Interference From Solar Panels For Space Vehicles," 2019 IEEE International Symposium on Electromagnetic Compatibility, Signal & Power Integrity (EMC+SIPI), 2019, pp. 487-492.

[8] Z. Chen et al., "Roadside Sensor Based Vehicle Counting Incomplex Traffic Environment," 2019 IEEE Globecom Workshops (GC Wkshps), 2019, pp. 1-5.

[9] W. Balid, H. Tafish and H. H. Refai, "Intelligent Vehicle Counting and Classification Sensor for Real-Time Traffic Surveillance," IEEE Transactions on Intelligent Transportation Systems, vol. 19, no. 6, pp. 1784-1794, June 2018.

[10] H. Zhu, S. Feng and F. Yu, "Parking Detection Method Based on Finite-State Machine and Collaborative Decision-Making," in IEEE Sensors Journal, vol. 18, no. 23, pp. 9829-9839, Dec, 2018.

[11] N. Wahlstrom and F. Gustafsson, Magnetometer modeling and validation for tracking metallic targets, IEEE Trans. Signal Process., vol. 62, no. 3, pp. 545-556, Feb. 2014.

[12] Y. Feng et al., "MagMonitor: Vehicle Speed Estimation and Vehicle Classification Through A Magnetic Sensor," IEEE Transactions on Intelligent Transportation Systems, vol. 23, no. 2, pp. 1311-1322, Feb. 2022.

[13] J. Xie et al., The simulations and experiments of the electromagnetic tracking system based on magnetic dipole model, IEEE Trans. Appl. Supercond., vol. 24, no. 3, pp. 1-4, Jun. 2014.

[14] Q. Wang, J. Zheng, H. Xu, B. Xu and R. Chen, "Roadside Magnetic Sensor System for Vehicle Detection in Urban Environments," IEEE Transactions on Intelligent Transportation Systems, vol. 19, no. 5, pp. 1365-1374, May 2018.

[15] Bao, Xu, Li, et al, "Traffic Vehicle Counting in Jam Flow Conditions Using Low-Cost and Energy-Efficient Wireless Magnetic Sensors," Sensors 2016. Vol. 16, Pages 1868.

Authorized licensed use limited to: XIDIAN UNIVERSITY. Downloaded on December 11,2024 at 05:22:40 UTC from IEEE Xplore. Restrictions apply.